IOPscience iopscience.iop.org

Home Search Collections Journals About Contact us My IOPscience

Heterostructure field effect transistors based on nitride interfaces

This article has been downloaded from IOPscience. Please scroll down to see the full text article.

2002 J. Phys.: Condens. Matter 14 3511

(http://iopscience.iop.org/0953-8984/14/13/309)

View the table of contents for this issue, or go to the journal homepage for more

Download details:
IP Address: 171.66.16.104
The article was downloaded on 18/05/2010 at 06:24

Please note that terms and conditions apply.

INSTITUTE OF PHYSICS PUBLISHING JOURNAL OF PHYSICS: CONDENSED MATTER

J. Phys.: Condens. Matter **14** (2002) 3511–3522 PII: S0953-8984(02)28773-1

Heterostructure field effect transistors based on nitride interfaces

J A Majewski, G Zandler and P Vogl

Physics Department and Walter Schottky Institute, Technische Universität München, Am Coulombwall, D-85748 Garching, Germany

Received 17 September 2001, in final form 29 January 2002
Published 22 March 2002
Online at stacks.iop.org/JPhysCM/14/3511

Abstract

A key property of the nitrides is the fact that they possess large spontaneous and piezoelectric polarization fields that allow a significant tailoring of the carrier dynamics and optical properties of nitride devices. In this paper, based on first-principles calculations of structural and electronic properties of bulk nitrides and their heterostructure, we investigate the potential of this novel material class for modern device applications by performing self-consistent Monte Carlo simulations. Our studies reveal that the nitride based electronic devices have characteristics that predispose them for high power and high frequency applications. We demonstrate also that transistor characteristics are favourably influenced by the internal polarization induced electric fields.

1. Introduction

In recent years, huge progress in the III–V nitride technology has been achieved. Commercial efforts have focused mostly on the optoelectronic applications (short wave LEDs and laser diodes) of nitrides but also nitride based electrical devices have attracted considerable interest. Such devices are promising candidates for high power, high frequency applications, that can range from cellular phones and satellite communications (0.8–1.9 GHz) through direct broadcast satellite TV (11–19 GHz) to anticolliding radar (80 GHz). Already fabricated GaN transistors [1] exhibit breakdown voltages that are unreachable in devices based on other materials (see figure 1). The measured values of the cut-off frequencues f_t show that the average electron transit velocity is 1.3–1.4 $\times$ 10^7 cm s^{-1}. This results in the intrinsic f_t of order 100 GHz, and the breakdown voltage of 35 V, for a typical effective gate length of 0.20 μm [1]. The electric figure of merit of these transistors is the maximum microwave output power multiplied by the square of the maximum frequency yielding 10 db of power gain, multiplied by the load resistance. This figure of merit for nitride high electron mobility transistors (HEMTs) is about 50 times that of GaAs devices, and about twice that of SiC metal semiconductor field-effect transistors (MESFETs) [1]. However, the desirable range of 180–200 GHz has not been reached yet. In the present paper, we review our recent studies of the

 © 2002 IOP Publishing Ltd Printed in the UK

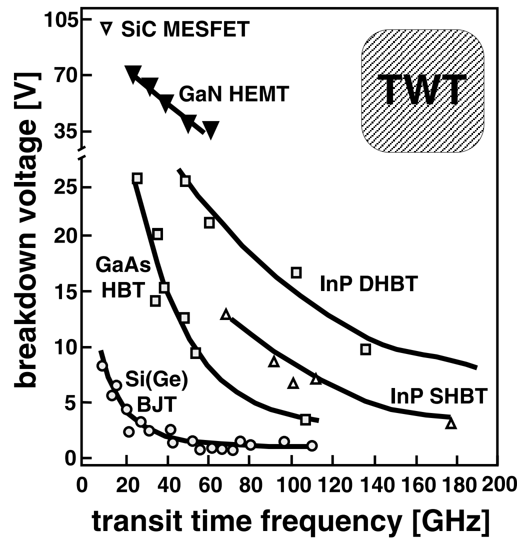

Figure 1. Breakdown voltage and transit time frequency of electron devices based on various materials. The region covered by travelling wave tubes (TWT) is also marked.

nitride electronic devices. We assess the potential of GaN/AlGaN heterostructure field effect transistors (HFET) for very high speed electronics by performing self-consistent ensemble Monte Carlo simulations.

The strong internal electric fields in nitrides that result from their strong pyro- and piezoelectric constants [2] have a dramatic effect on the electronic and optical properties in these systems. In the GaN or InGaN quantum wells, the electric field in the well causes the red shift of transition energies and strongly supresses the interband transitions [3]. This effect is generally considered as unfavourable for the optoelectronic devices based on multiple quantum wells [4]. On the other hand, the electric fields increase the electron and/or hole densities accumulated at the interfaces. This opens new possibilities for device engineering. In the present paper, we demonstrate how the pyro- and piezoelectric character of the nitrides can be utilized in the design of the novel HFETs. We show that the internal electric fields have a significant and favourable influence on the transistor characteristics.

The lack of detailed experimental data on transport parameters in nitride semiconductors is an obstacle in reliable device simulations. Therefore, we have performed extensive *ab initio* electronic structure calculations that provided us with the needed parameters. We have determined band offsets, the polarization induced charges at interfaces, the energies of all subsidiary conduction band minima relevant for high field transport, the effective masses of these valleys, and deformation potentials. The results of these studies will be given in section 2. We would like to point out that in spite of the fact that we focus in the present study on the electric devices, the results of section 2 are also of considerable importance for optical properties of nitride multi quantum wells and superlattices, since they provide reliable predictions concerning band offsets and polarization induced electric fields. Since the two-dimensional electron gas (2DEG) is the most important component of the HFETs, the theoretical studies of its properties are described in section 3. In section 4, the results of transport Monte Carlo calculations are presented. Finally, the paper is summarized in section 5.

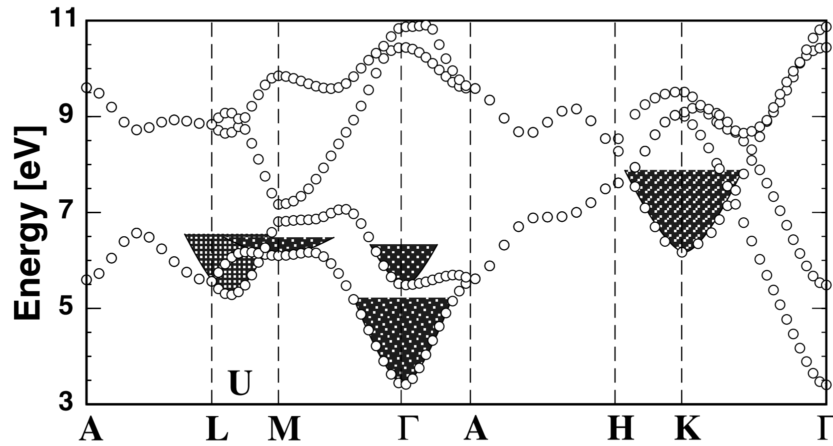

Figure 2. Conduction bands of wz–GaN as obtained from density functional calculations.

Table 1. The lowest conduction band minima in wz–GaN, and their positions relative to the conduction band bottom (in eV), effective masses (in units of m_0), and anisotropy parameters.

Valley	$E(\text{Valley}) - E(\Gamma_c)$	$m^*_\parallel$	$m^*_\perp$	α
Γ_c	0.0	0.18	0.20	0.6
U	1.87	1.43	0.33	0.2
Γ_c^3	2.08	2.17	0.28	0.3
M	2.68	2.62	2.12	0.2
K	2.77	0.65	0.40	−0.4

2. Theory of nitride bulks and their interfaces

In this section, we discuss the influence of the polarization fields on properties of nitride heterostructures. The present systematic theoretical studies of structural and electronic properties of heteroepitaxial AlN/GaN interfaces and homoepitaxial stacking faults [5], are based on a well established first-principles total-energy pseudopotential method within the local-density-functional formalism [6]. The band offsets, the charge accumulation at the polar interfaces of the junctions, and the interface electronic states have been investigated, taking fully into account the effects of lattice relaxation and electric polarization. Before we turn to the nitride heterostructures let us describe first the detailed electronic structure of the conduction bands in bulk wurtzite–GaN (wz–GaN), which is essential for the description of carrier dynamics in nitride devices.

2.1. Conduction bands in wurtzite–GaN

The wz–GaN exhibits rich structure of the conduction band minima (figure 2). The relevant valley effective masses and the nonparabolicity parameters α in wz–GaN predicted by the first-principles calculations are given in table 1. The conduction band minimum lies in the Γ-point. The second minimum lies in the U-point, which is placed on the ML line of the hexagonal Brillouin zone. We note that the sixfold degenerate U-point is equivalent to the three X valleys and three out of four L valleys of the zincblende Brillouin zone. In wurtzite–AlN (wz–AlN), the minimum lies in Γ-point and the conduction band edge effective mass equals 0.32 m_0.

2.2. Internal polarization fields in quantum wells

The space group $P6_3mc$ (C^4_{6v}) of wurtzite structure is compatible with a spontaneous polarization along the hexagonal c-axis. Therefore, the polarization can be of both pyroelectric and piezoelectric origin in wz–AlN and GaN, but only piezoelectric in the cubic phases. Whenever the polarization lies parallel to the growth direction, its change (divergence) across the interface is equivalent to an interface charge. Among the interfaces between GaN and AlN that we have studied, the [111] GaN/AlN, the [0001] GaN/AlN, and the stacking fault interface between the wurtzite– and zincblende–GaN (zb–GaN) interface are of this type, which may be termed 'polar'. In cases such as $[\bar{1}2\bar{1}0]$ GaN/AlN, $[0\bar{1}10]$ GaN/AlN, or [110] GaN/AlN, on the other hand, the polarization lies parallel to the interface and therefore does not give rise to a charge accumulation. We term those interfaces 'nonpolar'. A limiting case of this type is the cubic [001] GaN/AlN interface.

Most of the optoelectronic and electric nitride devices are based on the quantum wells. In such a structure, a thin layer of one semiconductor (e.g. GaN) constituting the well is embedded in another material (e.g. AlGaN). The vector of electric polarization in each material ($i = 1, 2$) can be written as $\boldsymbol{P}^{(i)} = \boldsymbol{P}_0^{(i)} + \chi^{(i)}\boldsymbol{E}^{(i)}$, where zero field polarization $\boldsymbol{P}_0^{(i)}$ consists of spontaneous and/or piezoelectric polarization, and $\chi^{(i)}$ is susceptibility of material 'i'. The most interesting case is when the polarizations $\boldsymbol{P}_0^{(i)}$ are perpendicular to the interfaces (like in the [0001] GaN/AlN system, for example). Then the divergence of the polarizations in two semiconductors gives rise to the polarization charges at the interfaces σ and further to the electric fields $\boldsymbol{E}^{(i)}$. The interface charge and electric field in the well are dependent on the boundary conditions imposed on the system. Here we consider three types of boundary conditions: (i) free standing system in vacuum, (ii) periodic boundary conditions, i.e. the potentials of the external surfaces of the cladding layers are equal, and (iii) neutralizing free charges σ_{fL} and σ_{fR} at the external surfaces. Further, we assume that the well has thickness l_1 and the two cladding layers on both sides of the well have thickness l_2 each. Using simple electrostatic arguments and considering the boundary conditions for the normal components of the electric displacements $D^{(i)} = 4\pi P_0^{(i)} + \epsilon_i E^{(i)}$ (ϵ_i dielectric constant) at four interfaces (two external surfaces and two internal interfaces) for the cases (i)–(iii), one obtains the interface polarization charges $\pm\sigma$ and electric fields in the well ($E^{(1)}$) and the cladding layers ($E^{(2)}$):

(i) $\quad \sigma = \frac{P_0^{(2)}}{\epsilon_2} - \frac{P_0^{(1)}}{\epsilon_1} \qquad E^{(1)} = -\frac{4\pi P_0^{(1)}}{\epsilon_1} \qquad E^{(2)} = -\frac{4\pi P_0^{(2)}}{\epsilon_2}$

(ii) $\quad \sigma = \frac{\left(P_0^{(2)} - P_0^{(1)}\right)(2l_2 + l_1)}{2l_2\epsilon_1 + l_1\epsilon_2} \qquad E^{(1)} = 4\pi\sigma\frac{2l_2}{2l_2 + l_1} \qquad E^{(2)} = -E^{(1)}\frac{l_1}{2l_2}$

(iii) $\quad \sigma = \frac{P_0^{(2)} - P_0^{(1)}}{\epsilon_1} \qquad E^{(1)} = 4\pi\sigma \qquad E^{(2)} = 0.$

Note that the relation $E^{(1)} - E^{(2)} = 4\pi\sigma$ holds in all three cases. In the case (iii), the free surface charges that cause the electric field in the cladding layer to vanish are $\sigma_{fL} = -\sigma_{fR} = P_0^{(2)}$. In the case (ii), the fields $E^{(1)}$, $E^{(2)}$, and the interface charge σ tend to the corresponding quantities from the case (iii), if the cladding layer thickness increases to infinity ($l_2 \to \infty$). For semiconductors with very similar dielectric constants ($\epsilon_1 \approx \epsilon_2$), like in the case of AlGaN/GaN quantum wells, the interface polarization charges are independent of the boundary conditions at the external surfaces. Then, the quantum well with neutralized surface charges (i.e. $E^{(2)} = 0$) can be well simulated in supercell calculations with periodic boundary conditions.

2.3. GaN/AlN heterostructures

In the following, we consider strained GaN layers that are grown pseudomorphically on cubic or wz–AlN substrate. For cubic heterostructures, we consider [001], [110], and [111], and for

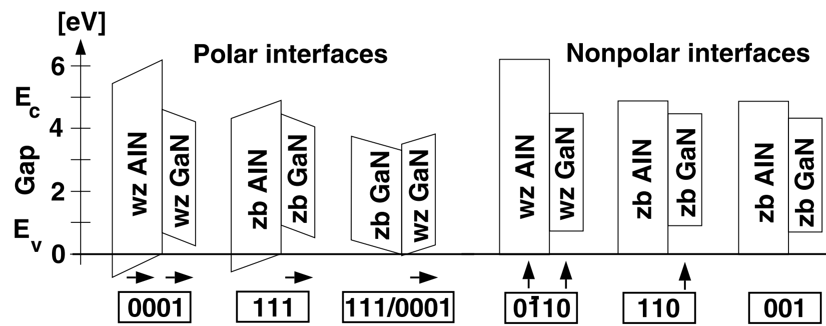

Figure 3. Predicted band lineups for several AlN/GaN interfaces. The growth direction is given in boxes beneath each interface. The arrows indicate the direction of the spontaneous or strain-induced piezoelectric polarization. Polar interfaces possess an interface charge. The corresponding electric field induces a band bending that is indicated schematically.

the wurtzite heterostructures [0001], $[0\bar{1}10]$, and $[\bar{1}2\bar{1}0]$ growth directions, respectively. In the case of stacking fault interfaces, we assume the growth axis to be the hexagonal *c*-axis ([0001] in wurtzite, [111] in zincblende).

Computationally, we have modelled all of these interfaces by supercells containing up to 40 atoms (for $[0\bar{1}10]$ and $[\bar{1}2\bar{1}0]$ wurtzite structures). All atomic positions in the unit cell have been optimized by minimizing the total energy via the Hellmann–Feynman forces. The length of the supercell was determined by minimizing the stress tensor component along the growth direction. Based on these first-principles calculations, we find that the charges induced at the interfaces and VBOs are insensitive to the lattice constant along the growth direction, but highly sensitive to the atomic relaxation at the interface (e.g. the VBO for the relaxed [0001] GaN/AlN interface is 0.4 eV smaller than for the unrelaxed one). The lattice relaxation near the interface reduces the interface charge approximately by a factor of two.

2.4. Valence band offsets and interface charges

The calculated band lineups [7] of the studied heterostructures are depicted in figure 3. It is interesting to note that all calculated VBOs for AlN/GaN heterostructures are of the order of 0.7–0.9 eV and are insensitive to the polar/nonpolar character of the interface. Thus, the macroscopic electric fields do not grossly alter or modify the intrinsic band offsets. The presently predicted VBOs agree very well with recent experimental data [8, 9], but not with some core-level photoemission data that suggest an extremely high VBO of 1.36 eV [10]. The large difference between conduction band offsets in cubic and wz–GaN/AlN heterostructures is a consequence of the indirect energy gap ($\Gamma \rightarrow X$) in cubic AlN that is 1.4 eV smaller than the direct gap in wz–AlN. In GaN stacking fault (zb–GaN/wz–GaN) the VBO is equal to 0.04 eV, whereas in AlN stacking fault (not shown in figure 3) the VBO is equal to 0.02 eV. All studied GaN/AlN interfaces and stacking faults are of type I, with the valence band lying higher and the conduction band being lower in GaN, and zincblende phase of the stacking fault, respectively.

The calculated charges at the polar interfaces are equal to 0.010 and 0.006 C m^{-2} for [0001] wz–AlN/wz–GaN and [111] zb–AlN/zb–GaN heterostructures, respectively. The large charges accumulated at the stacking fault interfaces (i.e. 0.009 and 0.003 C m^{-2} for AlN and GaN stacking faults, respectively) result mainly from the spontaneous dielectric polarization of the hexagonal phase, whereas the strain-induced piezoelectric contribution is negligible.

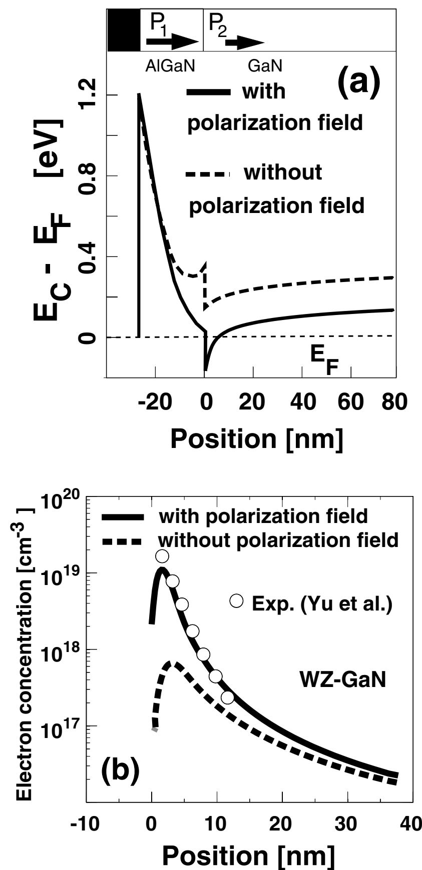

Figure 4. Calculated results for a $Al_{0.15}Ga_{0.85}N$/GaN heterostructure with (full curves) and without (dashed curves) spontaneous and piezoelectric fields. A homogeneous n-doping background of 10^{16} cm^{-3} throughout the structure has been assumed. (*a*) Selfconsistently computed conduction band edge profile along the growth direction. (*b*) Calculated electron density in comparison with published experimental values.

The presently calculated charges compare well (the difference amounts to 15–20%) with results obtained from electrostatic arguments, in which the bulk values of the spontaneous polarization, and piezoelectric constants [2] have been used. The stacking faults can generate a persistent photoconductivity and they can be tuned to act either as excitonic traps or luminescence centres, depending on the width of the cubic layer.

Our calculations reveal the existence of large internal electric fields in the nitride hetero- and homo-junctions. The influence of these electric fields on the properties of the electronic devices will be presented in subsequent sections.

3. 2DEG in AlGaN/GaN single heterostructures

As discussed in section 2, the electric polarization in nitride structures induces the polarization charge at the heterostructure interface. The 2DEG emerges at the interface with positive polarization charge. To study the transport properties of the 2DEG, we focus on a single $Al_{0.15}Ga_{0.85}N$/GaN heterostructure (see figure 4) first. The heterostructure consists of a tensile

strained 30 nm thick $Al_{0.15}Ga_{0.85}N$ and a Ga-face (i.e. with spontaneous polarization towards the substrate) the relaxed 300 nm thick GaN layer. In AlGaN layer, there is polarization of both pyro- and piezoelectric origins, while the GaN layer contains the pyroelectric moment only. We assume that there are some compensating charges at the surface and the nucleation layer. The polarization charge at the $Al_{0.15}Ga_{0.85}N$/GaN interface has been taken to be 6×10^{12} cm^{-2}, which interpolates between a recent experimental value [11] 4×10^{12} cm^{-2} and the theoretical value 8×10^{12} cm^{-2} calculated for full compensation.

Figure 4 depicts the self-consistent band edge and density profiles along the growth direction obtained from the coupled one-dimensional (1D) Schrödinger and Poisson equations. The Poisson equation includes all interface charges that result from the polarization fields. As shown in figure 4, the polarization induced positive interface charge causes a stronger confinement of 2D electron channel and an increase in the channel density by more than an order of magnitude. This is consistent with the experimental values for this layer structure [11].

Furthermore, we have performed ensemble Monte Carlo calculations for drift mobilities along the channel that forms parallel to the interface. The inter- and intra-subband-scattering rates [12] have been determined consistently with the confined electronic channel states. We find excellent agreement between experimental and calculated temperature dependent mobilities [12], consistent with the high channel densities reported for these devices [11, 13]. We would like to stress that such agreement strongly supports the existence of the strong pyroelectric polarization fields. For channel densities exceeding 10^{13} cm^{-2}, we predict a phonon limited drift mobility for 2D electrons close to 2000 cm^2 V^{-1} s^{-1} for high quality interfaces, in good agreement with recent data on such structures [14].

4. Monte Carlo simulations of nitride devices

Before we turn to the heterostructure based transistors, let us briefly discuss the transport properties of bulk nitrides.

4.1. Bulk transport properties of GaN and AlN

In our Monte Carlo transport calculations, we have used band parameters deduced from the electronic structure calculations described above and have taken into account scattering rates for ionized impurity, intra- and intervalley phonon scattering, acoustic, piezoelectric, polar optical phonon and alloy scattering. The resulting electron drift velocities (see figure 5) at room temperature in bulk GaN both at low and high fields are in good agreement with other published theoretical results [15]. At high fields, GaN, AlN and InN show a saturation velocity ($\sim 1.5 \times 10^7$ cm s^{-1} at 1 MV cm^{-1}) that is twice as high as in GaAs. For AlN, the heavier effective mass leads to considerably lower drift velocities at low fields. These results indicate that one can achieve much higher transit time frequencies in sub-micron nitride devices than in GaAs ones.

4.2. Characteristics of AlGaN/GaN HFETs

To study the influence of polarization fields on device characteristics, we have performed self-consistent 2D Monte Carlo simulations of various nitride based heterostructure devices. The results for HFET based on InGaN quantum well have been reported previously [7, 16]. It has been found that the polarization field pushes the electrons closer to the gate contact and therefore increases the transconductance. Furthermore, this confining effect improves the turn-off behaviuor of the device considerably.

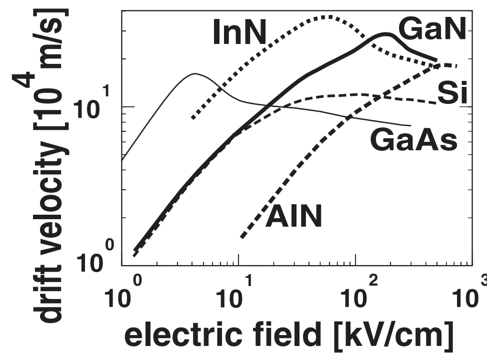

Figure 5. Calculated electron drift velocities of GaN, AlN, and InN in comparison with GaAs and Si.

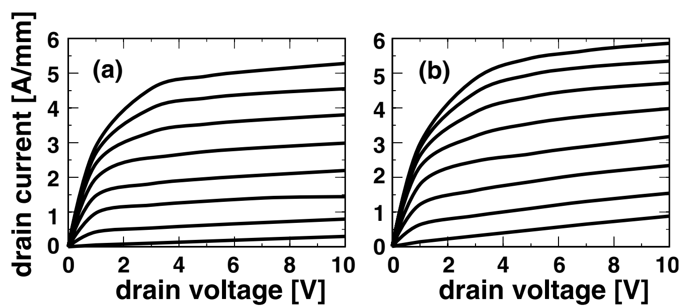

Figure 6. Drain current characteristics for HFET with gate lengths 300 nm (*a*) and 150 nm (*b*), as obtained from Monte Carlo simulations for $Al_{0.30}Ga_{0.70}N$/GaN HFET with the source–gate and gate–drain spacings equal to 275 and 500 nm, respectively. The various gate voltages are given in steps of 1 V and begin with -8.4 eV (the lowest line).

Here, we present results of Monte Carlo simulations for the standard design HFETs consisting of the slightly p-type doped GaN film and 25 nm wide undoped barrier of $Al_{0.30}Ga_{0.70}N$. These HFETs, owing to the strong spontaneous and piezoelectric polarizations, yield a high density of 2DEG ($\sim 10^{13}$ cm^{-2}) without intentional doping. It turns out to be favourable, since initial doping decreases electron mobility and increases gate tunnel leakage [1]. For an ideal interface, the low field channel mobility was found to be 1700 cm^2 V^{-1} s^{-1}. In this paper we report simulation results for transistors with gate length ranging from 150 to 300 nm and various source–gate (275–600 nm) and gate–drain (475–1200 nm) distances, which correspond to the parameters of experimental structures. The polarization induced interface charge has been estimated to be 1.6×10^{13} cm^{-2}. For the 'standard device', the source–gate and the gate–drain spacings have been chosen to be 275 and 500 nm, respectively. The current–voltage characteristics for this standard device with gate lengths of 150 and 300 nm are depicted in figure 6. As a consequence of the high channel densities and high drift velocities, the drain current is very large and increases only moderately with decreasing gate length. Further, we find out that the increase of source–gate spacing decreases the drain current, whereas, increased gate–drain distance influences the current only in the region of low voltage V.

The simulations predict the maximum transconductance to be roughly 900 S m^{-1} (see figure 7), which is a factor of two larger than the transconductance of currently realized transistors.

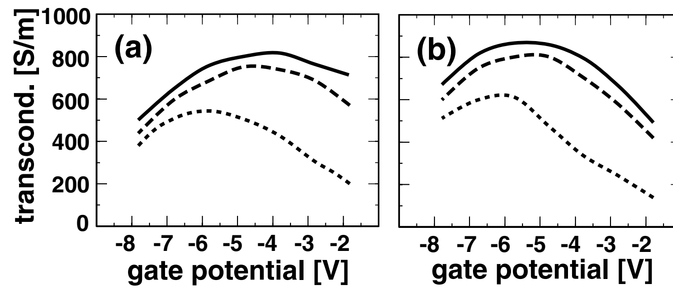

Figure 7. Calculated transconductance as a function of gate voltage for $Al_{0.30}Ga_{0.70}N$/GaN HFET (source–gate and gate–drain spacings are equal to 275 and 500 nm, respectively) with two different gate lengths (*a*) 300 nm, (*b*) 150 nm for three drain voltages equal to 1 V (dotted curve), 3 V (dashed curve), and 10 V (continuous curve).

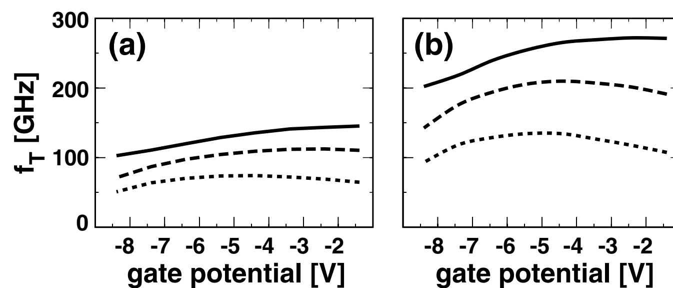

Figure 8. Calculated transit time frequencies as a function of gate voltage for $Al_{0.30}Ga_{0.70}N$/GaN HFET (source–gate and gate–drain spacings are equal to 275 and 500 nm, respectively) with two different gate lengths (*a*) 300 nm, (*b*) 150 nm for three drain voltages equal to 1 V (dotted curve), 3 V (dashed curve), and 10 V (continuous curve).

The results for transit time frequency, calculated from average channel velocity and the effective gate length, are presented in figure 8. The present Monte Carlo calculations predict average channel velocities exceeding 2×10^5 m s^{-1} for gate lengths below 200 nm. The transit time scales almost with the inverse of the effective gate length and can reach 250 GHz in the systems studied. This shows, that velocity overshoot effects play only a minor role in these HFETs. It is much larger than extrinsic transit times measured in experimental structures ($\sim$40 GHz).

We investigated the sensitivity of the transit time frequency onto other layout quantities of the device. The results are depicted in figure 9 for HFET with constant gate length of 300 nm. The curve labelled (a) shows the transit time frequency of the standard device described above. By increasing the source spacing from 275 to 600 nm, we find that the maximum transit time frequency decreases from 140 to 130 GHz (curve b in figure 9). Such a moderate decrease of the transit time frequency is a consequence of the high density and high mobility of the electrons in the source–gate part of the channel. A further decrease of the transit time frequency is found by increasing additionally the gate–drain spacing from 500 to 1200 nm. This results in lower effective channel fields and consequently to a reduction of the drift velocity in the channel, causing the observed decrease of the transit time frequency (curve c in figure 9) These effects become clearly even more pronounced for a less ideal device with lower channel mobility of 1000 cm^2 V^{-1} s^{-1} and a lower channel density of 10^{13} cm^{-2} (curve d in figure 9).

Very similar characteristics have been also calculated for the HFET with $Al_{0.83}In_{0.17}N$ quantum well and identical geometry parameters as in the HFET described above.

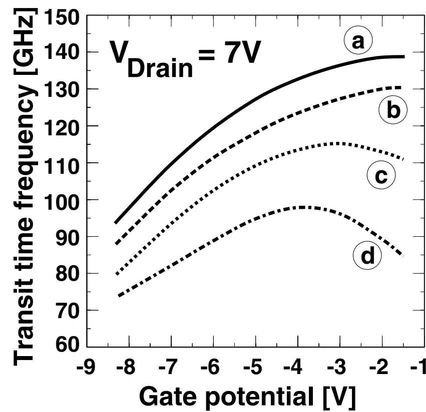

Figure 9. Calculated transit time frequencies as a function of gate potential for various AlGaN/GaN HFETs as described in the text. The drain voltage is equal to 7 V.

In conclusion, we predict excellent high frequency and power performance for wide-gap nitride based HFETs with gate lengths of the order of 200 nm.

4.3. Theoretically designed inverted HFET

Polarization induced internal fields can be effectively utilized to tailor devices with optimal potential barriers towards the substrate. Indeed, we have theoretically designed the following inverted HFET structure that should yield high channel densities and an excellent turn-off behaviuor. On top of a relaxed GaN buffer, there is a 12 nm thick strained $Al_{0.40}Ga_{0.60}N$ layer. The inner part (8 nm) of this layer is highly n-doped with 1.9×10^{19} cm^{-3}. The remaining part of the barrier is moderately doped with 10^{17} cm^{-3} carriers. On top of this layer, there is a 30 nm GaN (n-doped with 4×10^{16} cm^{-3}). The gate is assumed to be recessed in order to achieve a small gate to channel separation of 14 nm. In this HFET, we assume the opposite polarity of the structure as in the previous example, i.e. we have N-face GaN film with spontaneous polarization directed outward from the substrate. The GaN is assumed to be field free, whereas two GaN/AlGaN interfaces have opposite interface charges equal to $\pm 2 \times 10^{13}$ cm^{-2}. The calculated band edge profile, together with the confined electron density is shown in figure 10(*a*) at midgate position.

As can be seen from figure 10, the polarization induced field produces a high potential barrier of approximately 3 eV towards the substrate. This has two major consequences. First, the highly doped AlGaN barrier gets completely depleted and all electrons are strongly confined in the channel that forms at the interface with the top GaN layer. Secondly, the high barrier completely suppresses the leakage current across the AlGaN barriers up to high voltages. We predict excellent electrical characteristics for such devices. In the present example, we find drain currents exceeding 3000 A m^{-1} and a transconductance that lies well above 1000 S m^{-1}. We note that the thickness of the AlGaN barrier layer and its doping level must be chosen carefully in order to avoid the formation of parasitic hole channels.

5. Conclusions

In conclusion, pyro- and piezoelectrical polarizations must be taken into account in order to explain experimentally observed mobilities and densities in nitride heterostructures. They are

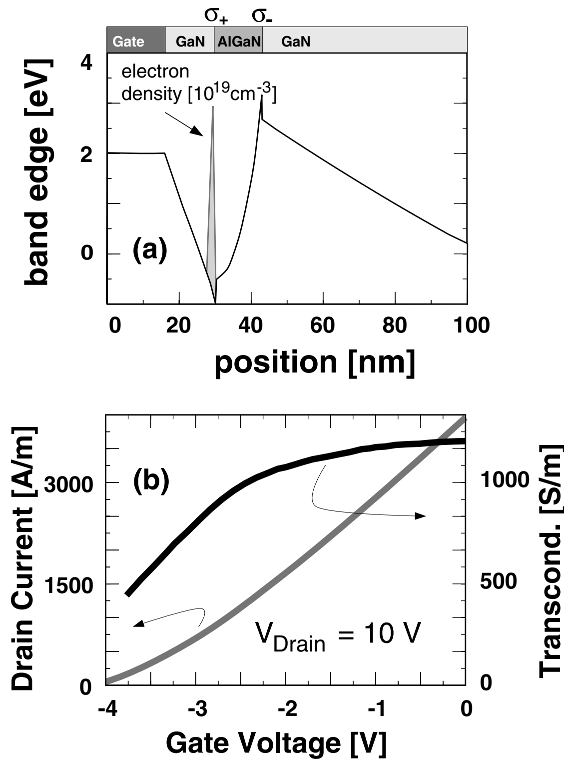

Figure 10. Monte Carlo results for a 300 nm gate length inverted $GaN/Al_{0.40}Ga_{0.60}N$ HFET. (*a*) Selfconsistent band edge profile for -1 V gate voltage and 10 V drain voltage. The channel electron density is indicated schematically. (*b*) Drain current and transconductance versus gate voltage at 10 V drain voltage.

crucial for device performances and offer a unique possibility to design novel high power high frequency heterostructure transistors. The nitride based HFETs have potential to substitute the travelling wave tubes that are commonly used nowadays for high power and high frequency applications.

Acknowledgments

The authors acknowledge fruitful discussions with Oliver Ambacher and Vincenzo Fiorentini. This work has been supported by the Deutsche Forschungsgemeinschaft (Project SFB 348).

References

[1] Eastman L F *et al* 2001 *IEEE Trans. Electron Devices* **48** 479
[2] Bernardini F, Fiorentini V and Vanderbilt D 1997 *Phys. Rev.* B **56** 10 024
[3] Leroux M, Grandjean N, Laügt M, Massies J, Gil B, Lefebvre P and Bigenwald P 1998 *Phys. Rev.* B **58** 13 371
[4] Nardelli M B, Rapcewicz K and Bernholc J 1997 *Appl. Phys. Lett.* **71** 3135
[5] Wu X H, Brown L M, Kapolnek D, Keller S, Keller B, DenBaars S P and Speck J S 1996 *J. Appl. Phys.* **80** 3228
[6] Städele M, Majewski J A and Vogl P 1997 *Phys. Rev.* B **56** 6911
Majewski J A, Städele M and Vogl P 1996 *MRS Internet J. Nitride Semicond. Res.* **1** 30
[7] Zandler G, Majewski J A and Vogl P 1999 *J. Vac. Sci. Technol.* B **17** 1617

[8] Martin G, Botchkarev A, Rockett A and Morkoç H 1996 *Appl. Phys. Lett.* **68** 2541
[9] Martin G, Strite S, Botchkarev A, Agarwal A, Rockett A, Morkoç H, Lambrecht W R L and Segall B 1994 *Appl. Phys. Lett.* **65** 610
[10] Waldrop J R and Grant R W 1996 *Appl. Phys. Lett.* **68** 2879
[11] Yu E T, Sullivan G J, Asbeck P M, Wang C D, Qiao D and Lau S 1997 *Appl. Phys. Lett.* **71** 2794
[12] Oberhuber R, Zandler G and Vogl P 1998 *Appl. Phys. Lett.* **73** 818
[13] Wu Y F, Keller B P, Kapolnek D, Kozodoy P, DenBaars S P and Mishra U K 1996 *Appl. Phys. Lett.* **69** 1438
[14] Gaska R, Yang J W, Osinsky A, Chen Q, Khan M A, Orlov A O, Snider G L and Shur M S 1998 *Appl. Phys. Lett.* **72** 707
[15] Bhapkar U V and Shur M S 1997 *J. Appl. Phys.* **82** 1649
O'Leary S K, Foutz B E, Shur M S, Bhapkar U V and Eastman L F 1988 *Solid State Commun.* **105** 621
[16] Zandler G, Majewski J A, Städele M, Vogl P and Compagnone F 1997 *Phys. Status Solidi* b **204** 133